18TH WORLD CONFERENCE ON EARTHQUAKE ENGINEERING
WCEE2024
MILAN

MILAN, ITALY
30TH JUNE - 5TH JULY 2024

www.wcee2024.it

GENERATION OF SYNTHETIC GROUND MOTIONS FOR GEOTHERMALLY INDUCED EARTHQUAKES

A. Kumawat[1], S. Keil[2], F. Taddei[1] & G. Müller[1]

[1] Technical University of Munich, TUM School of Engineering and Design, Chair of Structural Mechanics, Munich, Germany, aditi.kumawat@tum.de, francesca.taddei@tum.de, gerhard.mueller@tum.de

[2] Ludwig-Maximilians-Universität München, Department of Earth and Environmental Sciences, Munich, *Germany,* s.keil@lmu.de

Abstract: *With the rise of geothermal energy as a sustainable energy option, concerns about geothermally induced earthquakes have emerged, particularly with regard to infrastructure safety. This paper introduces a semi-analytical approach for generating synthetic ground motions in the context of geothermally induced micro-seismic events designed to address the lack of experimental ground motion data. The ground motion generation methodology is based on the layered half-space analysis developed using prior research available in this area. The technique is applied to a geothermal power plant in the east of Munich, Germany, where two seismic events of local magnitude* $M_L \approx 2.0$ *were recorded in 2016. The synthetic ground motions are simulated using the soil and source parameters relevant to this particular site.*

The findings reveal that velocities across various sensor directions display significant reductions with increasing distance from the epicenter, primarily attributed to radiation damping in the soil medium. The maximum velocities recorded in the simulations consistently remained below the 5mm/s threshold set by DIN4150-3, thereby highlighting the minimal potential for structural damage. Noteworthy from a computational perspective, the generation of synthetic ground motions using this approach exhibited remarkable efficiency, especially when contrasted with the numerical methods available in the open literature on wave-propagation simulation. Future work will refine the presented model by optimizing source and layer parameters to align more closely with recorded free-field data.

1 Introduction

Geothermal energy has become increasingly recognized for its potential as a sustainable and renewable energy source. While it offers several advantages, its extraction has been linked to geothermally induced earthquakes, causing concern in both scientific and local communities [Megies and Wassermann (2014), Küperkoch et al. (2018)]. Although relatively few and minor in scale, such seismic disturbances have raised concerns about infrastructure safety.

The limited availability of ground motion data due to a limited number of induced events hampers the research on the effects of geothermally induced seismic activity on the seismic safety of the built environment. The open literature is available on the simulation of seismic wave-propagation simulation, which can model 3D complex geometries of the soil medium to evaluate the seismograms [Käser et al. (2009), Keil et al. (2022)]. Although those tools and methodologies for generating seismic data offer high accuracies, they often demand substantial computational resources, posing challenges in efficiency and accessibility. Considering the scarcity of the available ground motion data for induced events and the computational inefficiencies of the available

wave-propagation simulation techniques, developing a simplified and fast approach for synthetic ground motion generation is essential.

In this paper, the synthetic ground motions are generated using a semi-analytical approach for layered half-space analysis. This methodology, as proposed by Singla and Gupta (2019), builds upon the initial work of Pei et al. (2008, 2009). The further sections of this paper briefly discuss the methodology details of the soil profile, discuss source parameters, and provide brief insights into the seismic event characteristics associated with a geothermal power plant facility in the outer Munich area in Germany. The results offer a comprehensive perspective on the synthetic ground motions produced for a single seismic event observed at various locations.

2 Methodology

The formulation adopted in this research has been adopted from the study by Singla and Gupta (2019) and Pei et al. (2008). The following sections briefly describe the characteristics of the soil medium and source parameters used for this study.

2.1 Layered Half-Space

The soil medium is assumed to comprise $(N+2)$ layers. Each of these layers is homogeneous and isotropic, exhibiting consistent material properties throughout its thickness. The layers are in direct contact with each other and are free from the body forces. Figure 1 shows the schematic diagram of the considered half-space model. The thickness, density, shear modulus, S-wave velocity, P-wave velocity, and depth are represented for the jth layer as h_j, ρ_j, μ_j, β_j, α_j, and d_j, respectively. The layer $(N+2)$ represents the half-space with $h_{N+2} \to \infty$ and $d_{N+2} \to \infty$. The source is located at the interface of layer J and layer $(J+1)$ at a depth d_J from the epicenter at the origin. It is assumed here that the material properties (thickness, density, shear modulus, and wave velocities) of these adjacent layers are identical, which simplifies the problem's boundary conditions.

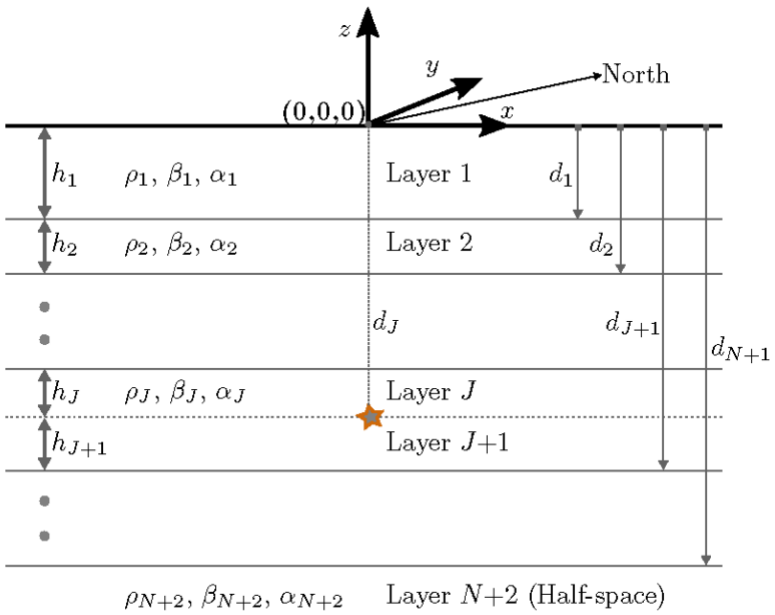

Figure 1: Layered half-space with $N+1$ layers plus underlying half-space with the source located in the Jth layer.

2.2 Source Parameters

The source is defined as a fault characterized by its strike, ϕ_f, dip-angle δ, slip λ, and an infinitesimal area $d\Sigma$, as illustrated in Figure 2. A slip $D(t)$ acts parallel to the fault plane, depicted by a half-sine pulse with a duration of T and an amplitude of D_0, also seen in Figure 3. The frequency domain of the surface translational displacement, $\boldsymbol{u}(x, y, \omega)$, is derived from the frequency-domain slip function $D(\omega)$ and the surface translational

displacement field $\boldsymbol{u}_g(x, y, \omega)$,

$$\mathbf{u}(x, y, \omega) = \hat{D}(\omega)\mathbf{u}_g(x, y, \omega), \tag{1}$$

where,

$$\begin{aligned}\mathbf{u}_g(x, y, \omega) = \quad & -\mu_J \left[\cos\lambda \left\{-\sin\delta \left(\frac{\partial \mathbf{g}_x}{\partial y} + \frac{\partial \mathbf{g}_y}{\partial x}\right)\right.\right. \\ & \left. + \cos\delta \left(\frac{\partial \mathbf{g}_x}{\partial d_J} + \frac{\partial \mathbf{g}_z}{\partial x}\right)\right\} \\ & + \sin\lambda \left\{-\sin 2\delta \left(\frac{\partial \mathbf{g}_y}{\partial y} - \frac{\partial \mathbf{g}_z}{\partial d_J}\right)\right. \\ & \left.\left. + \cos 2\delta \left(\frac{\partial \mathbf{g}_z}{\partial y} + \frac{\partial \mathbf{g}_y}{\partial d_J}\right)\right\}\right] \mathrm{d}\Sigma\end{aligned} \tag{2}$$

where ω is the angular frequency, and the terms $\boldsymbol{g}_x$, $\boldsymbol{g}_y$, and $\boldsymbol{g}_z$ are the frequency domain Green's function. The procedure to obtain those Green's functions have been elaborated in the study by Singla and Gupta (2019).

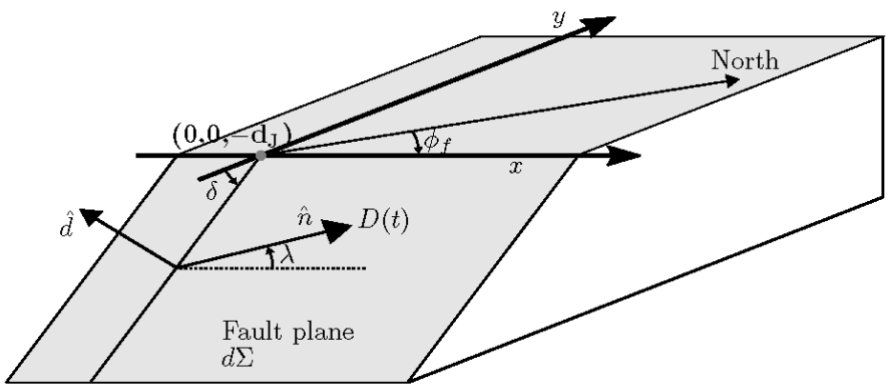

Figure 2: Source model for a fault located at the depth d_J with infinitesimal area $d\Sigma$ and strike, ϕ_f, dip-angle δ, slip λ.

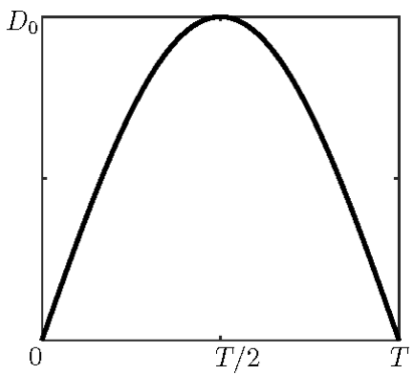

Figure 3: Slip function $D(t)$ represented as a half-sine pulse of duration T and amplitude D_0.

3 Event and Soil Data

In this research, the event and soil data are sourced from the studies conducted by Megies and Wassermann (2016) and Keil et al. (2022), respectively. Their studies are centered on a site situated to the east of Munich. Notably, in 2016, this site witnessed two seismic occurrences, each with a local magnitude of approximately M_L ≈2.0. Figure 4 offers a map pinpointing the site of the associated geothermal power plant (GPP). Additionally, the figure shows the three distinct recording stations: POI01, POI02, and POI03. These stations were situated at distances of 1.55 km, 5.6 km, and 3.3 km from the seismic events' epicenter, respectively.

Additionally, the depth d_J of the seismic source is based on the depth of the reservoir. The depth can be further refined on account of the depths of both the injection and production wells, as detailed in the work by Megies and Wassermann (2016). Summarizing the key parameters from the source that this study has considered: d_J stands at 2.5 km, the strike ϕ_f is set at 70°, the dip-angle δ is 60°, and the slip λ is -20°.

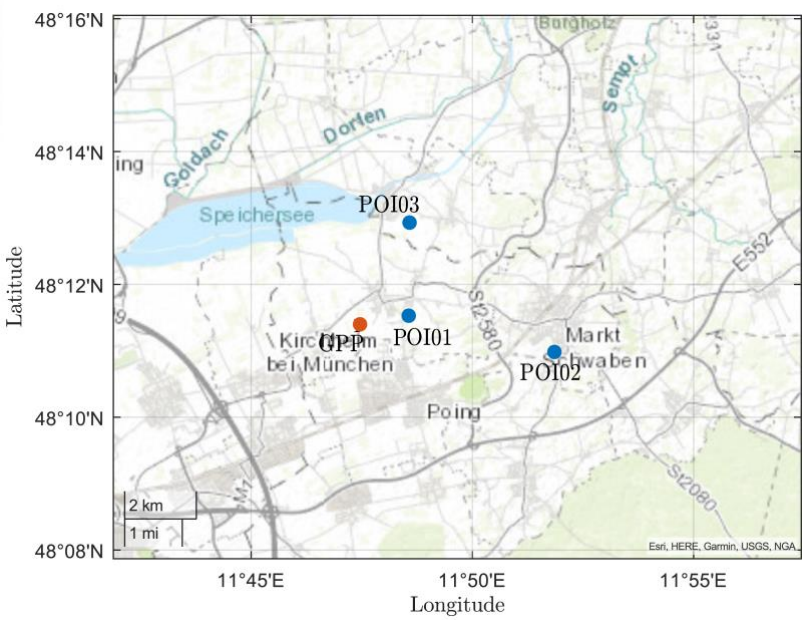

Figure 4: Map showing the geothermal power plant (GPP) and the seismic data recording stations POI01, POI02, and POI03 located at distances of 1.55 km, 5.6 km, and 3.3 *km from the epicenter.*

Furthermore, the 1D soil profile for Poing is detailed in Figure 5. The dotted curves show the S-wave velocity, β, P-wave velocity α, and soil density ρ up to a depth of 5515 m adopted by Keil et al. (2021, 2022). However, as the methodology used in this study requires uniform material properties per layer, the soil profile has been averaged over six layers plus half-space, as shown by the solid curves in Figure 5. The soil profile shows a Vs30 of 350 m/s. The β profile increases from 350 m/s to 3526 m/s, the α increases from 1050 m/s to 6100 m/s, and the ρ values increase from 2300 kg/m^3 to 2900 kg/m^3. The following section presents the ground motions simulated for the above-described soil medium and source parameters.

4 Synthetic Ground Motion

In this section, simulations were conducted to generate of the surface wave field for an earthquake with a local magnitude of $M_L = 2.0$. This local magnitude was subsequently converted into the moment magnitude, denoted as M_w [Grünthal und Wahlström (2003)],

$$M_w = 0.67 + 0.56M_L + 0.046\,M_L^2. \quad (3)$$

Subsequently, the moment magnitude was further transformed into the seismic moment M_0 using the following equation,

$$M_0 = 10^{1.5(M_w+10.7)}. \quad (4)$$

Further, the slip function $D(t)$ has been simulated for a time period T =0.1 seconds, and it may further be noted that the seismic moment is related to the shear modulus of the Jth layer μ_J, magnitude of slip function D_0, and fault area $d\Sigma$ as follows,

$$M_0 = \mu_J D_0 d\Sigma. \quad (5)$$

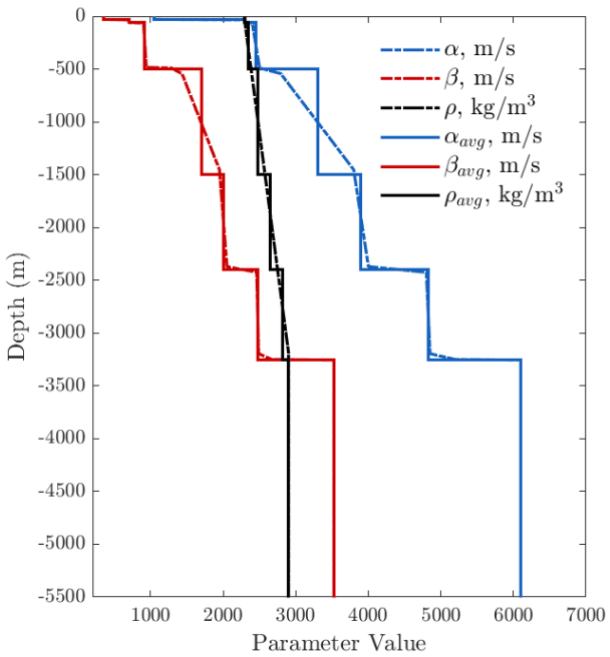

Figure 5: 1D soil profile for Poing representing original and averaged S-wave velocity β, P-wave velocity α, and soil density ρ. *Adopted from Keil et al. (2022).*

Figures 6 to 8 present the free-field velocities for the East-West (E-W), North-South (N-S), and vertical directions. Each figure displays the velocities evaluated at seven distinct locations, ranging from r =0.5 km to r =10 km from the epicenter. Each of the waveforms shown in Figures 6 – 8 is simulated for a frequency range of 0 – 10 Hz. This frequency range is chosen based on the significance of this range for induced events as discussed by Keil et al. 2022.

For all the simulated waveforms, it may be observed that as one moves further from the epicenter, there is a marked decrease in velocity values for each direction. Specifically, on comparing the points r =0.5 km and r =10 km, reductions of approximately 90%, 98%, and 93% were observed in velocities in the E-W, N-S, and vertical directions, respectively. This diminishing trend in velocity can be primarily attributed to the attenuation caused by radiation damping within the soil medium. Additionally, it is essential to highlight that as the distance from the epicenter grows, there is also an elongation in the time observed at the recording of

maximum displacement. This interval duration is related to the distance r (from the epicenter to the recording station) and the wave velocities therein the soil medium.

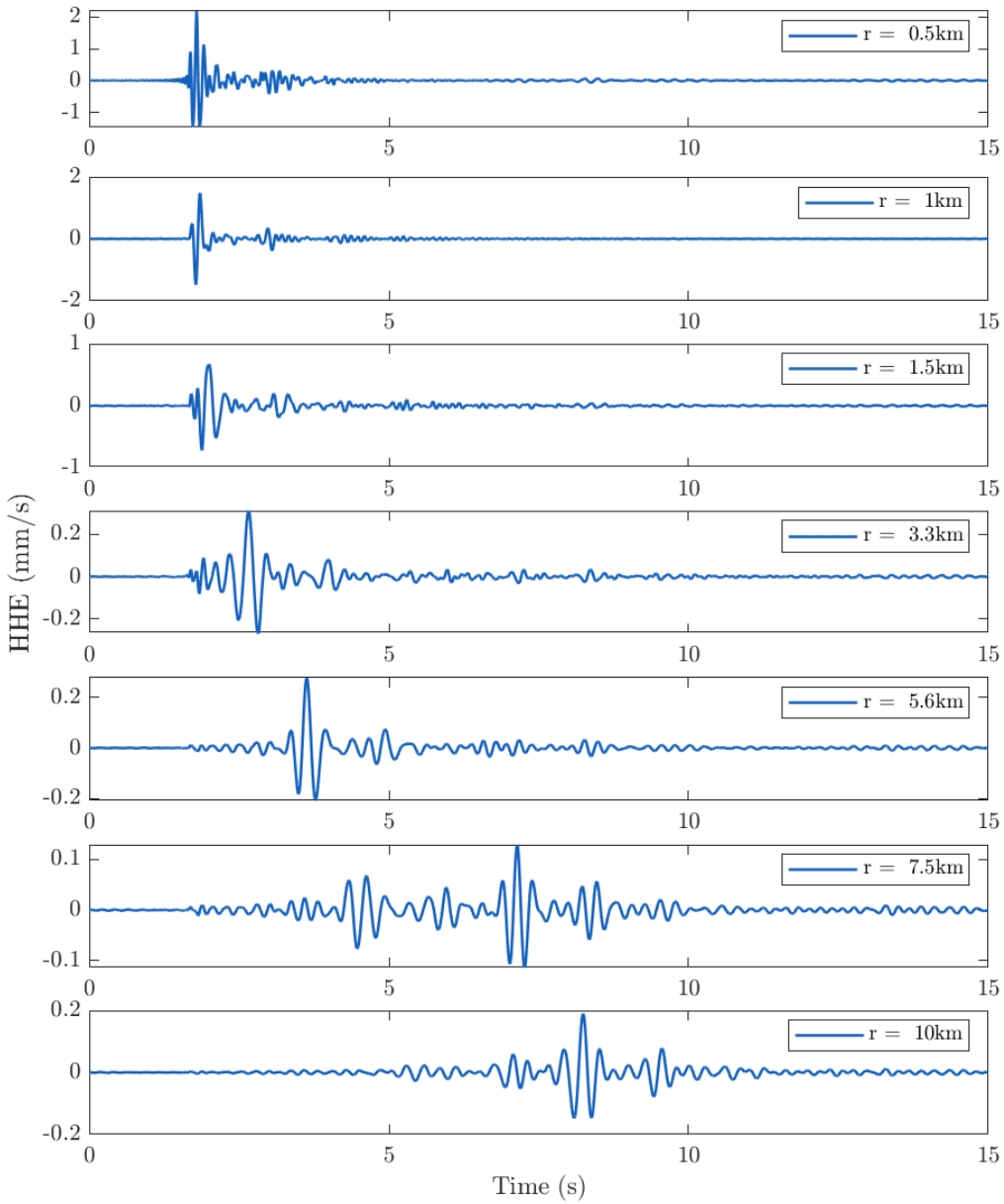

Figure 6: Simulated ground motions in the horizontal east-west sensor direction at various distances from the epicenter.

In addition to that, for the given source and medium characteristics, peak velocities recorded at r =0.5 km were 2.2 mm/s, 1.7 mm/s, and 0.2 mm/s for the E-W, N-S, and vertical directions, respectively. This variation in velocity amplitude across different directions at a singular location can be traced back to factors such as the orientation of the source and the positioning of the receiver. It is important to note that all the simulated free-field vibrations remained under the 5 mm/s threshold, a benchmark set by DIN4150-3 for evaluating structural damages.

From a computational standpoint, simulating frequency domain Green's functions within the 0 to 10 Hz frequency range took approximately 8 minutes. Conversely, evaluating time-domain waveform outcomes for a designated r value was achieved in roughly 60 seconds. These computations were executed on a 2x Intel

Xeon-Gold 6136 3GHz/12C computer with dual 12 processors. The relatively fast runtime of the presented methodology underscores its applicability in engineering contexts. Furthermore, although the representation of the soil medium is simplified to a 1D model, the approach is significantly faster than the contemporary approaches for ground motion generation, which utilizes a 3D model for soil medium, for example, the study by Keil et al. (2022).

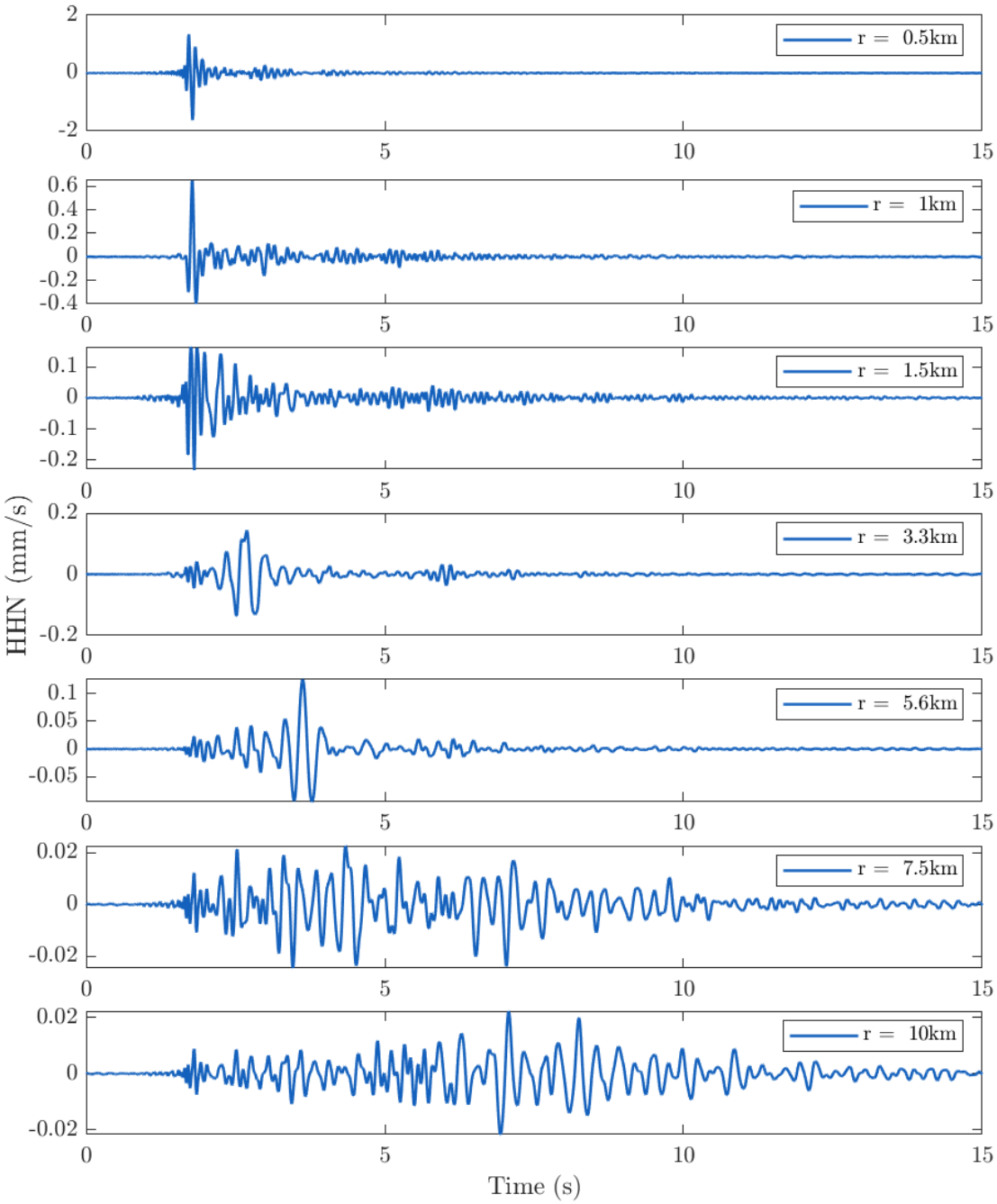

Figure 7: Simulated ground motions in the horizontal north-south sensor direction at various distances from the epicenter.

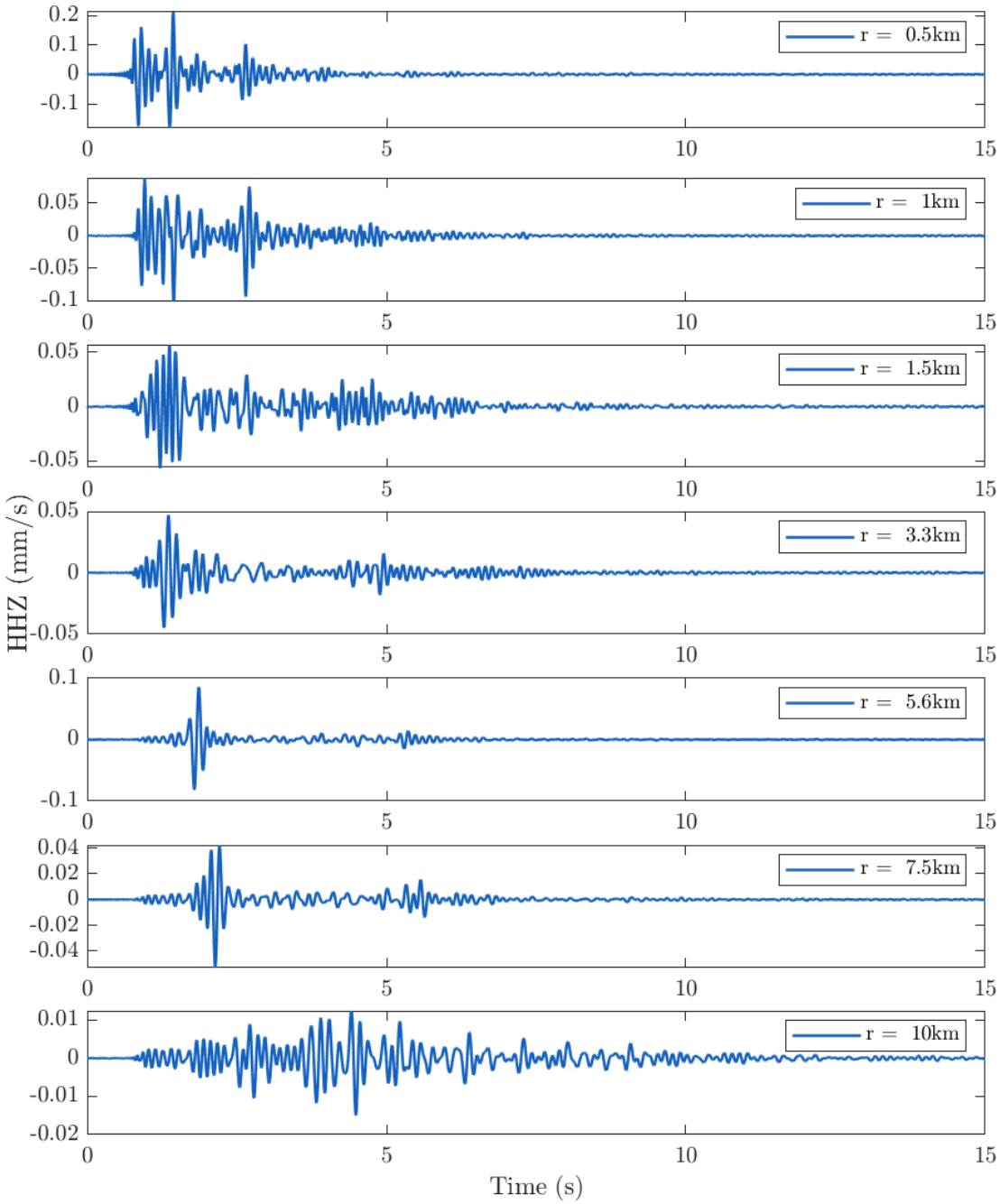

Figure 8: Simulated ground motions in the vertical direction at various distances from the epicenter.

5 Conclusion

This research provides a fast approach to simulated synthetic ground motions for the geothermally induced events in the absence of experimental data. The approach can be efficiently utilized for the in-depth exploration of seismic wave propagation in layered half-spaces. The soil medium and source parameters utilized in this study correspond to the geothermal facility located in the east of Munich. The analysis shows the behavior of free-field velocities across various sensor directions relative to the distance from the seismic event's epicenter. Notably, the study pinpointed significant velocity reductions due to factors such as radiation damping within the soil medium.

Moreover, while the simulated vibrations highlighted variations in velocity based on source orientation and receiver positioning, they all remained safely below the threshold set for structural damage assessment by

DIN 4150-3. The efficiency of the computational approach was further underscored by the exceptionally fast runtimes observed for evaluating Green's functions. Further research will involve optimizing the source and layer parameters to match the recorded free-field data.

6 Acknowledgements

The authors thank the Bavarian State Ministry for Science and Art (Bayerisches Staatsministerium für Wissenschaft und Kunst) for funding this research within the collaborative research project Geothermie Allianz Bayern (GAB).

7 References

Grünthal, G. and Wahlström, R., 2003. An Mw based earthquake catalogue for central, northern and northwestern Europe using a hierarchy of magnitude conversions. *Journal of seismology*, *7*, pp.507-531.

Käser, M., Castro, C., Hermann, V. and Pelties, C., 2010. SeisSol–a software for seismic wave propagation simulations. In High Performance Computing in Science and Engineering, Garching/Munich 2009: Transactions of the Fourth Joint HLRB and KONWIHR Review and Results Workshop, Dec. 8-9, 2009, Leibniz Supercomputing Centre, Garching/Munich, Germany (pp. 281-292). Springer Berlin Heidelberg

Keil, S., Wassermann, J. and Igel, H., 2021. Single-station seismic microzonation using 6C measurements. Journal of Seismology, 25, pp.103-114.

Keil, S., Wassermann, J. and Megies, T., 2022. Estimation of ground motion due to induced seismicity at a geothermal power plant near Munich, Germany, using numerical simulations. Geothermics, 106, p.102577.

Küperkoch, L., Olbert, K. and Meier, T., 2018. Long-term monitoring of induced seismicity at the Insheim geothermal site, Germany. Bulletin of the Seismological Society of America, 108(6), pp.3668-3683.

Megies, T. and Wassermann, J., 2014. Microseismicity observed at a non-pressure-stimulated geothermal power plant. Geothermics, 52, pp.36-49.

Megies, T. and Wassermann, J., 2016. Erste auswertung des erdbebens im raum Pliening/ Poing vom 07.12.2016 mit auswertung des nachbebens am 20.12.2016. Bayerischer Erdbebendienst.

Pei, D., Louie, J.N. and Pullammanappallil, S.K., 2008. Improvements on computation of phase velocities of Rayleigh waves based on the generalized R/T coefficient method. Bulletin of the Seismological Society of America, 98(1), pp.280-287.

Pei, D., Louie, J.N. and Pullammanappallil, S.K., 2009. Erratum to improvements on computation of phase velocities of Rayleigh waves based on the generalized R/T coefficient method. Bulletin of the Seismological Society of America, 99(4), pp.2610-2611.

Singla, V. K. and Gupta, V. K., 2019. Surface rotations due to kinematic shear dislocation point source in a multilayered elastic medium. Bulletin of the Seismological Society of America, 109(1), pp.433-447.

Vibrations in buildings - Part 3: Effects on structures. DIN 4150-3:2016-12. December 2016.